nature chemistry

Article

https://doi.org/10.1038/s41557-026-02177-8

Ligand-modulated metal–radical polarity match enables general 1,2-dicarbofunctionalization of ethylene

Received: 5 February 2026

Accepted: 12 May 2026

Published online: 10 June 2026

Check for updates

Zhexuan Lei[1], Chu Wang[1], Anwei Wang[1], Tao Liu[1], Zhe Dong[2] ✉, Weigang Zhang[1,3] ✉ & Jie Wu[1,4] ✉

Leveraging transition metal catalysis to direct multiple radical intermediates towards a single desired product offers many synthetic opportunities while presenting an important chemoselectivity challenge arising from selectivity in radical capture by the catalyst. How mechanistic design precisely tunes this selectivity remains limited, constraining the rational design of efficient catalytic systems. Here we demonstrate that the electronic bias of the radical intermediates and the ligand-modulated copper centre can be strategically harnessed to control the selectivity of copper-mediated radical capture. A strongly π-accepting terpyridine ligand modulates the electronic properties of the copper catalyst, enabling the selective capture of radical intermediates with complementary polarity through a metal–radical polarity-match mechanism. Building on this mechanistic framework, we have established a synthetically powerful, yet highly challenging ethylene 1,2-dicarbofunctionalization. This provides streamlined access to structurally diverse, medicinally relevant 1,2-dicarbofunctionalized ethanes that incorporate sp^3-, sp^2- and *sp*-hybridized carbogenic functional groups while offering mechanistic insights and design principles that facilitate the rational design of transition metal-catalysed radical transformations.

The merger of photoredox catalysis and transition metal (TM) catalysis has revolutionized synthetic radical chemistry by enabling new pathways to generate organometallic intermediates from radical precursors[1–5]. This synergy has sparked growing interest in reactions that engage multiple radical intermediates, unlocking transformations previously inaccessible through either catalytic platform alone[6–12]. For instance, combining intramolecular radical translocation and TM catalysis has enabled powerful remote C–H functionalization with excellent regiocontrol[13], while TM-catalysed radical functionalizations of unsaturated systems that proceed via radical addition enable the construction of multiple C–C or C–X bonds from simple building blocks[14]. Recently, the emergence of TM-catalysed radical cross-coupling has enabled selective bond formation between two independently generated radical intermediates[8–12]. Despite these advances, such transformations face a fundamental chemoselectivity challenge: the TM catalyst needs to selectively capture the desired carbon-centred radical among multiple competing transient intermediates to form the productive organometallic intermediate[15–17]. This issue becomes especially pronounced when radicals are generated through intermolecular relay processes or from distinct precursors (Fig. 1a, left).

[1]Department of Chemistry, National University of Singapore, Singapore, Republic of Singapore. [2]Department of Chemistry, Southern University of Science and Technology, Shenzhen, People's Republic of China. [3]College of Chemical Engineering, Nanjing Tech University, Nanjing, People's Republic of China. [4]National University of Singapore (Suzhou) Research Institute, Suzhou, People's Republic of China. ✉e-mail: dongz@sustech.edu.cn; wgzhang@njtech.edu.cn; chmjie@nus.edu.sg

https://doi.org/10.1038/s41557-026-02177-8

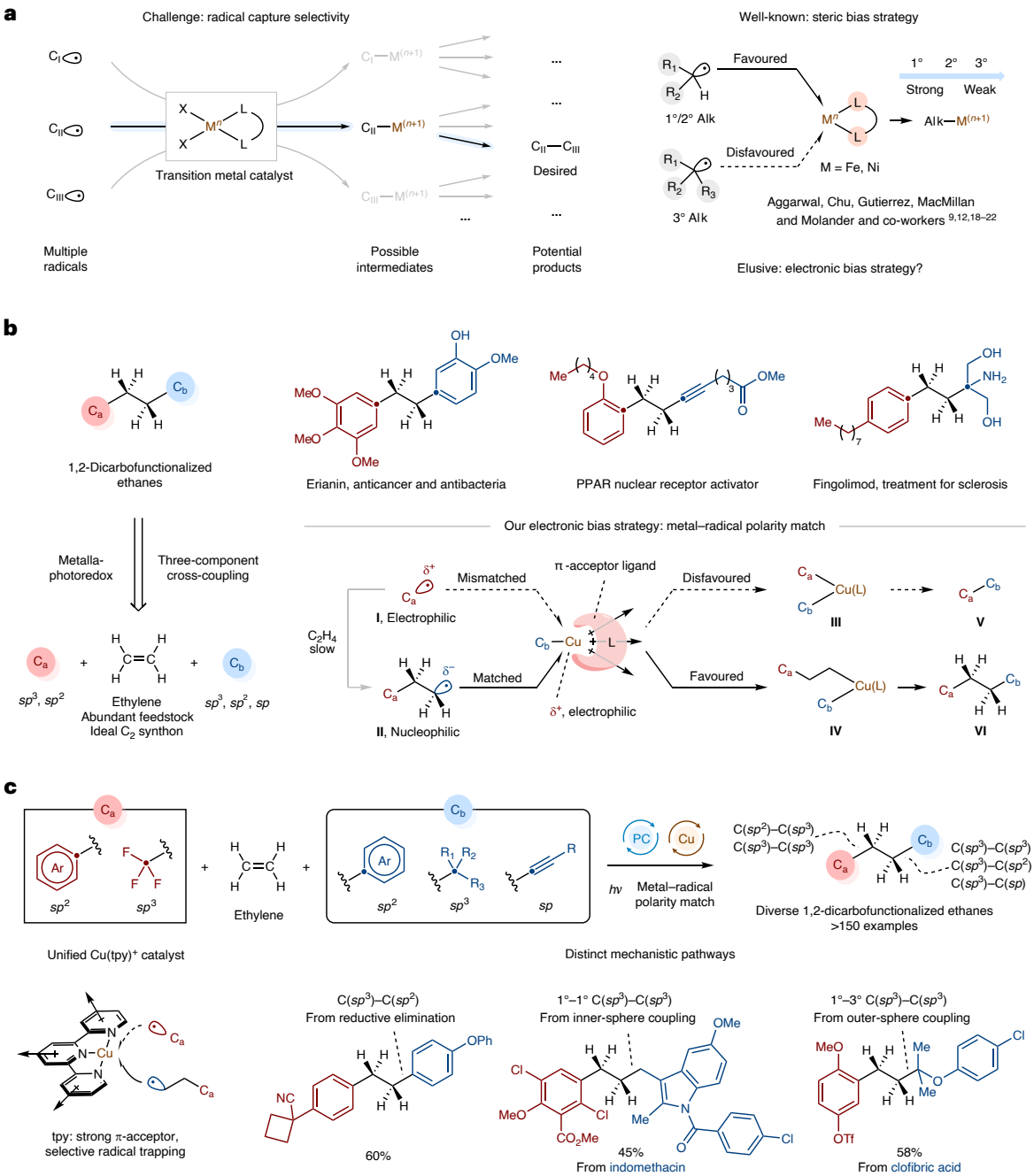

Fig. 1 | Ligand-modulated selective radical capture through metal–radical polarity match enables generalized photoredox/copper dual-catalysed 1,2-dicarbofunctionalization of ethylene. a, Challenge of radical capture selectivity and well-known strategy for selectivity based on steric bias[9,12,18–22]. **b**, 1,2-Dicarbofunctionalized ethanes accessed by three-component 1,2-difunctionalization of ethylene based on the electronic bias strategy. **c**, This work: a generalized 1,2-dicarbofunctionalization of ethylene enabled by unified photoredox/copper–tpy dual catalysis built upon metal–radical polarity-match mechanisms. M, metal; L, ligand; X, ligand; R, functional group; Alk, alkyl; PC, photocatalyst; PPAR, peroxisome proliferator-activated receptor; Ar, aryl; OTf, trifluoromethanesulfonyloxy; 1°, primary; 2°, secondary; 3°, tertiary.

A well-established strategy to achieve this radical capture selectivity relies on steric bias, exploiting the TM catalyst's preference for less sterically hindered alkyl radicals (Fig. 1a, right). In the TM-catalysed 1,2-difunctionalization of alkenes, for example, bulky tertiary alkyl radicals are employed as the initial species to minimize premature capture, promoting radical addition to the alkene and yielding a less hindered secondary radical that is more readily captured by the catalyst, thereby facilitating the desired three-component coupling[18–21]. MacMillan and co-workers demonstrated a similar steric principle in which a TM catalyst preferentially captures the less sterically hindered primary radical to form an alkyl–metal species that subsequently undergoes bimolecular homolytic substitution (S_H2) with a bulkier, more nucleophilic secondary or tertiary radical to achieve C(sp^3)–C(sp^3) coupling[9,12,21,22]. These steric-based strategies, while effective, leave the role of electronics in governing radical capture selectivity poorly understood[16,23].

Intriguingly, copper catalysts have been shown to distinguish between aryl and alkyl radicals through differences in the reversibility of radical capture and the metal's oxidation state[24], suggesting that electronic factors may indeed play a decisive role. Extensive

studies have also demonstrated that radical reactions often follow a 'polarity-match' principle, whereby radicals preferentially react with partners of complementary electronic character[25]. This principle has been shown to govern the selectivity in radical addition, atom transfer and homolytic substitution reactions[26]. We therefore reasoned that the electronic interplay between radical intermediates and the copper catalyst—modulated by the ligand's electronic properties—could be strategically harnessed for selective radical capture. Here we describe a 'metal–radical polarity-match' mechanism in which complementary polarity between radicals and the TM complex dictates radical capture preference and thus chemoselectivity. We applied this concept to unlock a general platform for ethylene 1,2-dicarbofunctionalization.

1,2-Dicarbofunctionalized ethanes are valuable scaffolds widely found in pharmaceuticals and natural products, with notable examples including erianin, sarpogrelate, chlorambucil and fingolimod (Fig. 1b and Extended Data Fig. 1). A survey of the Reaxys database[27] (July 2025) identified over 440,000 such compounds (when C_a is aryl), approximately 23% of which have reported pharmacological activities. The saturated C_2 linker, or ethane bridge, is a privileged structural element in fragment-based drug discovery, offering compact size, conformational flexibility and enhanced metabolic stability[28] (Extended Data Fig. 2). For instance, linking two arene fragments with a saturated C_2 linker has been shown to improve beta-secretase 1 (BACE-1) inhibitory potency more than 360-fold (Extended Data Fig. 2a)[29–32]. Given its abundance (over 300 million tonnes global annual production in 2024), ethylene is an ideal yet underused synthon for constructing such motifs. However, previous ethylene difunctionalization strategies were limited to 1,2-homodifunctionalization[33], relied on TM-catalysed migratory insertion that necessitates a prefunctionalized substrate or directing group[34–36], or a radical cascade strategy[37–39], limiting the synthetic scope.

Building on our long-standing interest in ethylene radical difunctionalization[33,37,38], we envisioned that a generalized ethylene 1,2-dicarbofunctionalization platform, where two carbogenic functional groups are installed across ethylene via metallaphotoredox catalysis, would enable access to this valuable chemical space with superior efficiency and modularity. Our mechanistic design draws inspiration from the metallaphotoredox-catalysed 1,2-difunctionalization of substituted alkenes[18–20,40–42]. As illustrated in Fig. 1b, an electrophilic carbon-centred radical **I**, generated by photoredox catalysis, undergoes radical addition to ethylene to form the first C–C bond; the resulting primary alkyl radical **II** is then captured by the TM catalyst to generate organometallic intermediate **IV**, which forges the second C–C bond to deliver the desired 1,2-dicarbofunctionalized ethane **VI**. However, achieving selective radical capture remains a formidable challenge owing to the intrinsic inertness of ethylene. Due to its gaseous nature and lack of substitution, the reactivity of ethylene towards radical addition (~10^3 M^{-1} s^{-1}) is lower than that of substituted alkenes (10^4–10^7 M^{-1} s^{-1})[43], while the capture of certain electrophilic radicals by the TM catalyst approaches diffusion control[44,45]. This severe kinetic mismatch makes radical **I** overwhelmingly prone to premature capture by copper, competitively generating the two-component by-product **V** rather than the desired three-component product[24,46,47].

The metal–radical polarity-match mechanism provides a direct solution: by employing a ligand-tuned, electron-deficient copper centre[48–50], the electrophilic radical **I** becomes a polarity-mismatched partner for capture, while the nucleophilic radical **II**—generated only after productive addition to ethylene—is kinetically favoured, funnelling reactivity towards the desired three-component pathway (Fig. 1b). In this work, we identified the strongly π-accepting ligand 2,2′:6′,2″-terpyridine (tpy) as critical for tuning the copper catalyst's electronic properties to enforce this selectivity and established a general photoredox/copper dual-catalysed platform for ethylene 1,2-dicarbofunctionalization (Fig. 1c). We found that the tpy ligand largely suppressed the capture of electrophilic radical **I** by the copper catalyst, while favoring the capture of nucleophilic radical **II**, consistent with the metal–radical polarity-match mechanism. Notably, aryl radicals, whose capture by TM catalysts is remarkably facile[24,46,47,51], even approaching diffusion-controlled for copper[44,45], were successfully engaged in the dicarbofunctionalization. Their direct capture by copper was effectively suppressed using tpy, while interception of the nucleophilic radical **II** remained efficient, directly validating the polarity-match principle. The $Cu(tpy)^+$ complex was found to operate across multiple coupling paradigms, enabling the incorporation of $C(sp^3)$, $C(sp^2)$ and $C(sp)$ building blocks through mechanistically distinct pathways—reductive elimination, inner-sphere alkyl–alkyl coupling or outer-sphere S_H2 substitution—depending on the nature of the coupling partner. When engaging $C(sp^3)$ partners, $Cu(tpy)^+$ can orchestrate three radical intermediates towards the desired product, exhibiting both electronic and steric discrimination.

Reaction discovery

1,2-Diarylethanes (bibenzyls) represent the most well-documented 1,2-dicarbofunctionalized ethane scaffolds[38], with notable bioactive examples such as erianin, sarpogrelate, pemetrexed, denzimol and polysignine. As a proof of concept for our mechanistic platform, we targeted their synthesis via copper-catalysed ethylene diarylation, in which an aryl radical precursor served as C_a while an arylboronic acid acted as C_b[52–54]. After an extensive survey of reaction conditions, we found that aryldibenzothiophenium (aryl-DBT) salt **1a**, readily prepared from unfunctionalized arenes, served as the optimal aryl radical precursor[55], with arylboronic acid **2a** as the coupling partner and a ruthenium-based photocatalyst proving essential owing to its matched redox potential and strong absorption in the visible-light region. Under these photoredox/copper dual-catalytic conditions, the desired 1,2-diarylethane **3a** was obtained in 60% yield (Fig. 2a). The proposed mechanism is shown in Extended Data Fig. 4.

Ligand screening revealed a pronounced ligand effect on both the three/two-component (**3a**/**4a**) selectivity and overall efficiency (Fig. 2a). Terpyridine (**L1**), a strongly π-accepting ligand[56], gave optimal results with exceptional selectivity (**3a**/**4a** > 99:1), while ligands bearing less electron-withdrawing heterocyclic motifs, such as one pyrazolyl unit (**L2**), two 4,5-dihydrooxazol-2-yl units (**L3**) and two pyrazolyl units (**L4**), led to markedly diminished selectivity and reactivity. Commonly used bidentate nitrogen-donor ligands (**L5**–**L8**), weaker π-acceptors due to narrower conjugation, performed poorly, producing **4a** as the dominant product. To quantify this trend, density functional theory calculations were performed to determine the energy gap between the highest-occupied molecular orbital (HOMO) and lowest-unoccupied molecular orbital (LUMO) of the corresponding copper complexes as a measure of the ligand's π-accepting capacity, with strong π-acceptors exhibiting low-lying π^* orbitals and hence a smaller HOMO–LUMO energy gap ($\Delta E_{HOMO-LUMO}$)[50]. An inverse correlation between $\Delta E_{HOMO-LUMO}$ and selectivity for **3a** was observed (Fig. 2a). $Cu(tpy)^+$ had the lowest $\Delta E_{HOMO-LUMO}$ of 2.91 eV and the best selectivity, while $Cu(\mathbf{L8})^+$ had the highest $\Delta E_{HOMO-LUMO}$ of 4.17 eV and the lowest **3a**/**4a** ratio (see Supplementary Sections 4.3 and 4.4 for details). This lowered LUMO energy enhances the electrophilicity of the copper centre, creating a kinetic preference for the capture of nucleophilic radical **II** over electrophilic radical **I**—directly consistent with the radical capture mechanism governed by polarity match.

We then examined the effect of ligand substituents on the selectivity (Fig. 2b). Modification of the tpy scaffold with electronically diverse functional groups (**L1**-**2** to **L1**-**7**) showed minimal impact on the ligand's π-accepting ability ($\Delta E_{HOMO-LUMO}$ = 2.78–2.99 eV), and all maintained excellent selectivity (>99:1). Furthermore, introducing sterically bulky groups onto the 2,6-bis(4,5-dihydrooxazol-2-yl)pyridine (**L3**) scaffold (**L9** and **L10**) did not improve selectivity, implying that steric effects play a limited role in modulating radical capture in this system.

https://doi.org/10.1038/s41557-026-02177-8

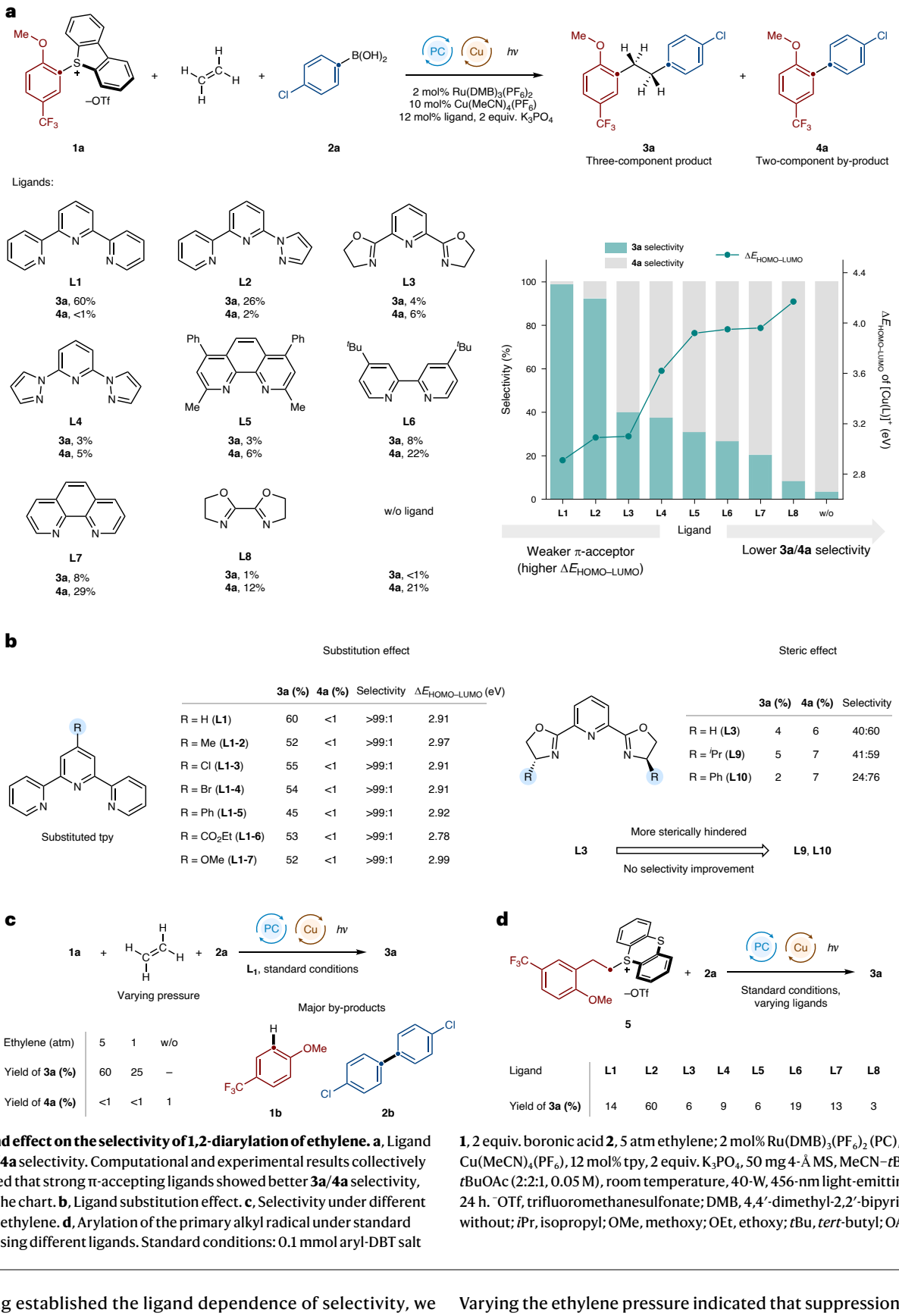

Fig. 2 | Ligand effect on the selectivity of 1,2-diarylation of ethylene. a, Ligand effect on **3a**/**4a** selectivity. Computational and experimental results collectively demonstrated that strong π-accepting ligands showed better **3a**/**4a** selectivity, as shown in the chart. **b**, Ligand substitution effect. **c**, Selectivity under different pressures of ethylene. **d**, Arylation of the primary alkyl radical under standard conditions using different ligands. Standard conditions: 0.1 mmol aryl-DBT salt **1**, 2 equiv. boronic acid **2**, 5 atm ethylene; 2 mol% $Ru(DMB)_3(PF_6)_2$ (PC), 10 mol% $Cu(MeCN)_4(PF_6)$, 12 mol% tpy, 2 equiv. K_3PO_4, 50 mg 4-Å MS, MeCN–*t*BuCN–*t*BuOAc (2:2:1, 0.05 M), room temperature, 40-W, 456-nm light-emitting diode, 24 h. $^-$OTf, trifluoromethanesulfonate; DMB, 4,4′-dimethyl-2,2′-bipyridine; w/o, without; *i*Pr, isopropyl; OMe, methoxy; OEt, ethoxy; *t*Bu, *tert*-butyl; OAc, acetate.

Having established the ligand dependence of selectivity, we turned to examine whether other reaction parameters contribute to the observed **3a**/**4a** selectivity. We first investigated whether high ethylene concentration would improve the selectivity by kinetically favouring radical addition over premature radical capture (Fig. 2c). Varying the ethylene pressure indicated that suppression of **4a** formation did not primarily depend on the concentration of ethylene. Biaryl **4a** was formed in only 1% yield even in the absence of ethylene, with the major by-products being 4-trifluoromethylanisole (**1b**), generated from hydrogen atom transfer to the aryl radical, and

4,4′-dichloro-1,1′-biphenyl (**2b**), formed by deborodimerization of **2a**. In contrast, ligands with inferior **3a**/**4a** selectivity (**L2**–**L8**) showed a strong dependence on ethylene pressure, with **L7** producing **4a** in over 40% yield in the absence of ethylene (see Supplementary Fig. 12 for details). Notably, the formation of **2b** confirmed that Cu(tpy)$^+$ remains competent for aryl–aryl bond formation under these conditions, indicating that the low yield of **4a** with **L1** reflects suppressed aryl radical capture rather than an inability to promote aryl–aryl coupling. We further probed the role of radical acceptor reactivity by conducting the diarylation reaction with styrene, a superior radical acceptor, under the standard conditions with different ligands. Across all the ligands tested, the three/two-component selectivity with styrene was markedly improved compared with ethylene (Extended Data Fig. 3 and Supplementary Fig. 15), highlighting that the selectivity advantage of tpy is specific to the challenging ethylene substrate and reflects its ability to discriminate between radical intermediates rather than simply benefiting from a more reactive acceptor.

We next investigated whether the inferior **3a**/**4a** selectivity observed with other ligands stems from their inability to promote C(sp^3)–C(sp^2) bond formation (step **IV** → **VI**, Fig. 1b), rather than from poor selectivity in radical capture. To probe this, 2-arylethylthianthrenium (TT) salt **5**, from which primary alkyl radical **II** is directly generated without requiring ethylene, was prepared and subjected to the standard diarylation conditions (Fig. 2d). All the ligands tested promoted C(sp^3)–C(sp^2) coupling to varying extents, confirming that bond formation competency is not the limiting factor. Crucially, **L2** and **L6**, which showed poor three-component selectivity (Fig. 2a), gave substantially higher two-component coupling yields (60% and 19%, respectively) than **L1** (14%), an inverse correlation that directly demonstrates that their failure in the three-component reaction does not stem from an inability to mediate C(sp^3)–C(sp^2) bond formation (see Supplementary Fig. 24 for details). Rather, it demonstrates that the poor selectivity with these ligands originates from their ineffective discrimination between radical intermediates **I** and **II**.

Collectively, these results establish that the ligand-modulated selective radical capture by the copper catalyst is the key factor in the exceptional performance of tpy (**L1**). The strongly π-accepting nature of **L1** renders the copper centre more electrophilic[57–59], which, according to the metal–radical polarity-match principle, kinetically favours the capture of nucleophilic alkyl radical **II** while disfavouring the mismatched capture of electrophilic aryl radical **I** (see Supplementary Fig. 11 for a detailed illustration). This polarity-guided discrimination directs the reactivity towards the three-component coupling pathway with outstanding selectivity (see Supplementary Section 4 for detailed discussions).

Having established the optimal reaction conditions with tpy as the most effective ligand, we next explored the substrate scope of the 1,2-diarylation protocol (Fig. 3). The mild conditions of this dual-catalytic system proved broadly tolerant of various functional groups, such as esters (3b, 3d, 3f, 3l, 3p, 3r, **3w** and **3x**), ketones (3c, 3e, **3t** and **3z**), cyanides (3i, 3k, **3u** and **3v**), triflate (**3g**), sulfonamides (**3n** and **3o**), sulfones (**3m** and **3aa**), amides (3l, **3q** and **3s**) and halogens (**3a**–3t, **3ad**–3af, **3aj** and **3ak**). Structurally complex and pharmaceutically relevant compounds were also compatible (**3p**–**3t**), highlighting the synthetic utility of this method for late-stage functionalization. In addition, this transformation displayed wide compatibility with both electron-poor (**3u**–**3aa**) and electron-rich (**3ab**–**3ad**) arylboronic acids, as well as heteroaromatic coupling partners (**3ai**–**3an**), further illustrating its robustness across electronically diverse substrates. More electron-rich aryl radical precursors generally afforded the product in moderate yields (3f, 3n, **3s** and **3t**), likely due to slower radical addition to ethylene due to reduced electrophilicity. Given the ubiquity of arene functionalities, which can be readily converted to aryl-DBT salts, the abundance of ethylene and the wide availability of arylboronic acids, this 1,2-diarylation reaction provides step-economic and modular access to a large library of 1,2-diarylethanes with rich structural diversity. To further demonstrate the synthetic utility, several bioactive compounds were directly assembled in a modular, step-economic manner (**3ao**–**3ar**; Fig. 3c). Notably, this approach stands in stark contrast to previously reported two-component strategies that required substantially longer synthetic sequences. The extended substrate scope is provided in Supplementary Fig. 2.

Expansion of the scope of carbogenic coupling partners

We then explored whether other carbogenic functional groups could be incorporated within the same paradigm, extending the reaction beyond diarylation. We first diversified the first carbogenic partner (C_a, Fig. 1b) by examining the 1-trifluoromethyl-2-arylation of ethylene using trifluoromethylsulfonium salt **6** as the trifluoromethyl radical precursor[60] (Fig. 4a). Under the established Ru photocatalyst/copper–tpy dual-catalytic system, the desired 1-trifluoromethyl-2-arylethane motif **7** was smoothly generated with both electron-poor and electron-rich arylboronic acids (**7a**–**7e**). Mechanistically analogous to the 1,2-diarylation, the reaction proceeds via addition of the initial trifluoromethyl radical to ethylene, followed by copper-catalysed arylation.

We next diversified the second carbogenic group (C_b). Specifically, we questioned whether alkynylation, a well-established copper-catalysed transformation of alkyl radicals[61–63], could be integrated into the ethylene dicarbofunctionalization framework. Replacing arylboronic acid **2** with terminal alkyne **8** under the same Ru photocatalyst/copper–tpy dual-catalytic system, we successfully established an ethylene 1-aryl-2-alkynylation reaction (Fig. 4b), providing modular access to 1-aryl-2-alkynylethanes, a scaffold widely present in bioactive molecules (Extended Data Fig. 1), from simple arenes, ethylene and alkynes. The proposed mechanism is illustrated in Extended Data Fig. 5. This dicarbofunctionalization exhibited broad functional group tolerance, compatible with a diverse range of terminal alkynes, including alkyl- (**9a**–9c, **9e** and **9f**), silyl- (**9d**), carbonyl- (**9g**) and aryl-substituted (**9h**) variants. The extended scope of the aryl- and trifluoromethyl-alkynylation of ethylene is presented in Supplementary Fig. 3.

Having achieved both C(sp^3)–C(sp^2) and C(sp^3)–C(sp) bond formation, we turned to the more challenging construction of C(sp^3)–C(sp^3) linkages—an increasingly important motif in drug discovery due to the three dimensionality and favourable pharmacokinetic properties of sp^3-rich scaffolds[64], yet a longstanding challenge in synthetic chemistry[65]. Unlike arylboronic acids and terminal alkynes, which engage copper through transmetalation to generate organocopper intermediates (Extended Data Figs. 4 and 5), analogous alkyl transmetalation to copper is rare[66], necessitating an alternative mechanistic approach. Recent advances have shown that iron and nickel catalysts can mediate radical alkyl–alkyl cross-coupling through steric discrimination[9–12], whereas analogous copper-catalysed transformations remain underdeveloped. We therefore envisioned constructing the C(sp^3)–C(sp^3) bond through Cu(tpy)$^+$-mediated radical cross-coupling, wherein established polarity-match selectivity is complemented by steric discrimination to differentiate between the two alkyl radical partners.

Aliphatic carboxylic acids were selected as the C(sp^3) coupling partner given their abundance and well-established capacity to generate alkyl radicals via decarboxylation[67]. Under photoredox conditions, the decarboxylation of acid **10** generates an alkyl radical that undergoes selective copper-catalysed cross-coupling with primary alkyl radical **II** derived from addition to ethylene, delivering the target C(sp^3)–C(sp^3) product **11**. Systematic reaction optimization using aryl-DBT salt **1** and aliphatic carboxylic acid **10** revealed that the Cu(tpy)$^+$ complex again emerged as the optimal catalyst. However, the ruthenium photocatalyst had to be replaced by an acridinium-type photocatalyst, which possesses a more oxidative excited state essential for decarboxylative generation of the alkyl radical from **10** (Fig. 5a). In this three-radical

https://doi.org/10.1038/s41557-026-02177-8

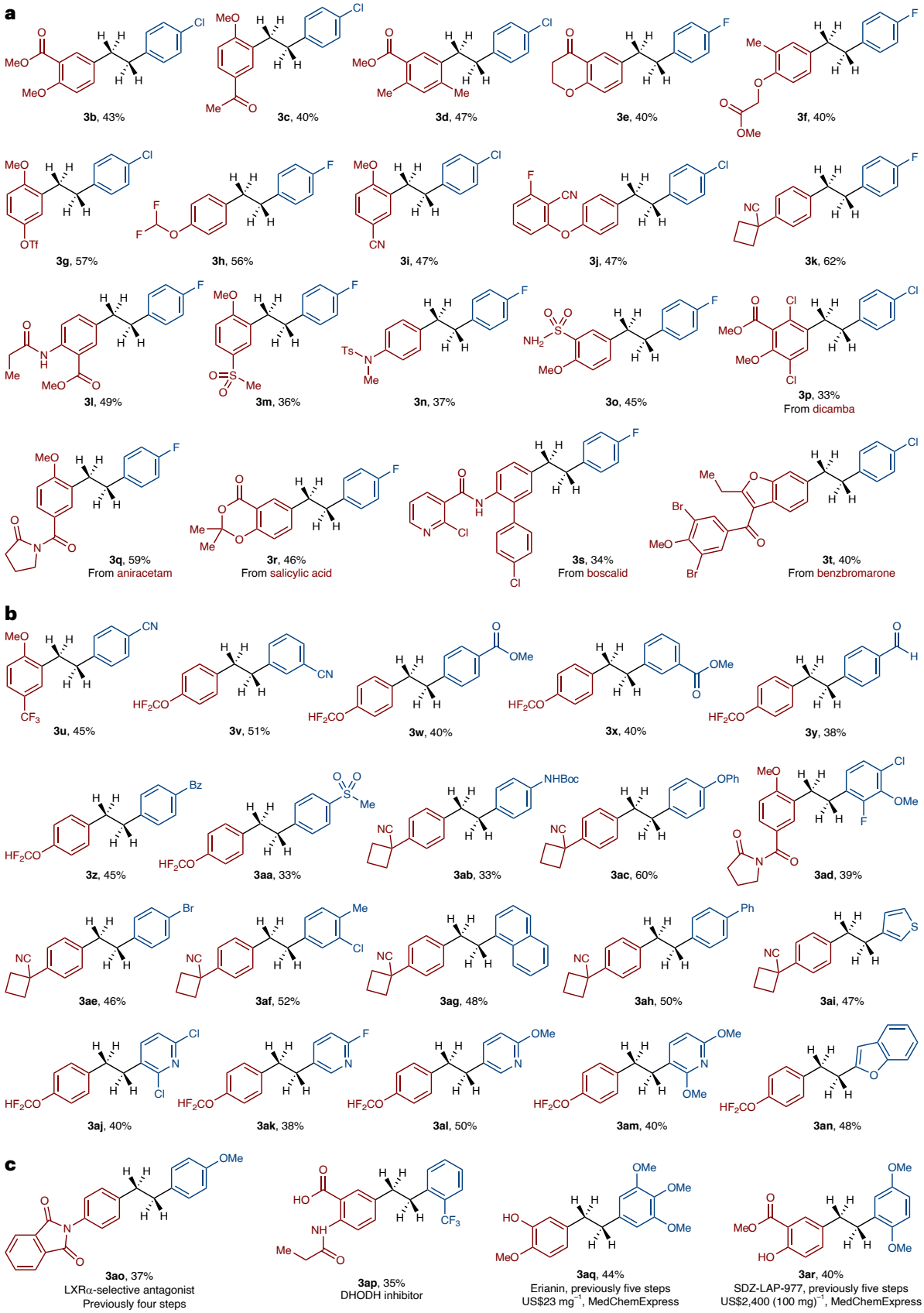

Fig. 3 | Substrate scope of ethylene 1,2-diarylation. a, Scope of the aryl-DBT salt. **b**, Scope of arylboronic acids. **c**, Modular and step-economic synthesis of bioactive 1,2-diarylethanes. Reactions were performed under the standard conditions and isolated yields are reported. Ts, *p*-toluenesulfonyl; Bz, benzoyl; Boc, *tert*-butyloxycarbonyl; OPh, phenoxy; LXRα, liver X receptor α-isoform; DHODH, dihydroorotate dehydrogenase.

https://doi.org/10.1038/s41557-026-02177-8

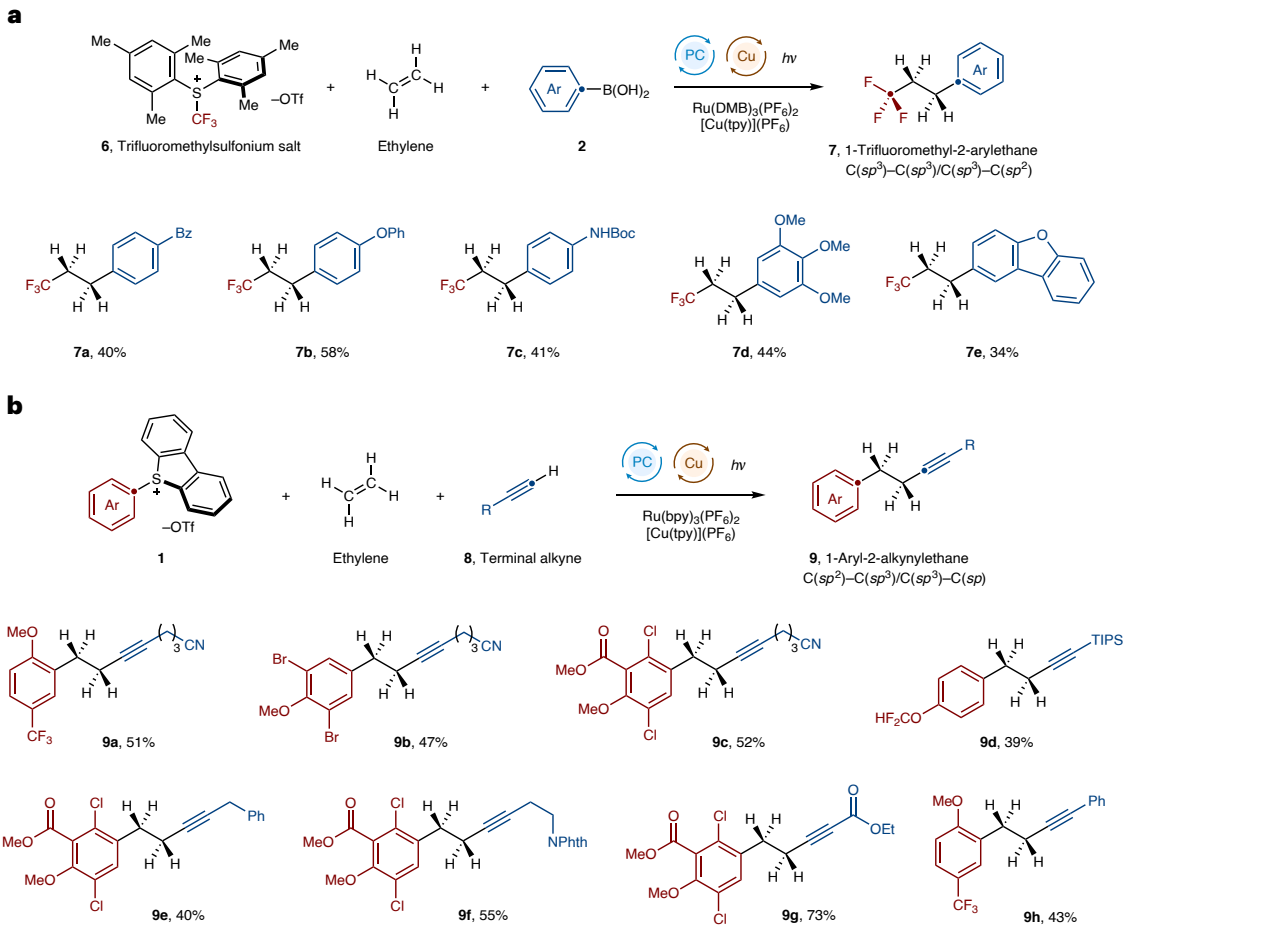

Fig. 4 | Extension of reaction to other carbogenic coupling partners. a, 1-Trifluoromethyl-2-arylation of ethylene. **b**, 1-Aryl-2-alkynylation of ethylene. The reactions were performed under modified standard conditions (Supplementary Section 5.1) and isolated yields are reported. TIPS, triisopropylsilyl; NPhth, phthalimidyl.

system, $Cu(tpy)^+$ enforces selectivity at two distinct levels: polarity match governs the capture of nucleophilic primary alkyl radical **II** over electrophilic aryl radical **I**, while steric bias simultaneously disfavours capture of the bulkier secondary and tertiary alkyl radicals derived from the acids, together directing all three radical intermediates towards the desired product. The resulting primary alkyl–copper species then forms a $C(sp^3)$–$C(sp^3)$ bond with the unbound alkyl radical through either an inner-sphere reductive elimination (when primary arylacetic acid derivatives are used, vide infra) or an outer-sphere S_H2 substitution pathway. The proposed mechanism is illustrated in Extended Data Fig. 6.

Study of the substrate scope of the 1-aryl-2-alkylation of ethylene revealed that primary, secondary and tertiary aliphatic carboxylic acids are all suitable coupling partners (Fig. 5b). Among primary acids, arylacetic acid derivatives (**11a**–**11n**) proved especially efficient, with benzylic radical intermediates undergoing facile TM capture[16] and productive inner-sphere reductive elimination. Aryl- and heteroarylacetic acid derivatives, including complex drug molecules such as indomethacin (**11m**) and isoxepac (**11n**), were also compatible, underscoring the synthetic utility of this transformation. In contrast, unactivated primary acids gave lower yields with substantial homocoupling of the two primary alkyl radicals generated in situ, reflecting the inherent difficulty in differentiating sterically and electronically similar primary alkyl radicals.

Secondary carboxylic acids proved broadly compatible with the selective dicarbofunctionalization reaction (**11o**–**11ae**). Several complex drug molecules containing secondary carboxylic acid motifs, including ibuprofen (**11o**), ketoprofen (**11p**), naproxen (**11q**) and loxoprofen (**11r**), participated in the transformation effectively. Also, in contrast to primary acids, unactivated secondary acids were viable substrates (**11s**–**11ae**). Interestingly, when cyclic acids were employed, the overall efficiency showed a strong dependence on ring size. Reactants with smaller ring sizes afforded lower yields (**11v**–**11x**), likely due to the decreased nucleophilicity of the corresponding alkyl radical, consistent with the proposed S_H2 mechanism. Tertiary carboxylic acids were also viable substrates, producing all-carbon quaternary centres, a highly desirable yet synthetically challenging motif. Both phenylacetic acid derivatives (**11af** and **11ag**) and unactivated acids (**11ah**–**11an**) furnished the targeted 1-aryl-2-alkylethanes smoothly in good to synthetically useful yields. Notably, 1-methylcyclobutane-1-carboxylic acid gave the desired product in 45% yield (**11ai**), while secondary cyclobutanecarboxylic acid delivered only 18% yield (**11v**). This increased reactivity is attributed to the higher nucleophilicity of the tertiary 1-methylcyclobutyl radical compared with the secondary analogue, further supporting the proposed S_H2 pathway. For the extended substrate scope, see Supplementary Fig. 4.

Application to substituted alkenes and 1,3-butadiene

We next explored whether this protocol could be extended to substituted alkenes **12** (Extended Data Fig. 3). Styrene can be readily functionalized under the standard ethylene 1,2-diarylation conditions, delivering 1,1,2-triarylethane scaffolds (**13a**–**13e**). 1,3-Butadiene also proved to be a competent substrate, affording the corresponding 1,4-diarylated products exclusively as *trans* alkenes (**13f**–**13i**). Propylene, another abundant gaseous feedstock, underwent smooth

https://doi.org/10.1038/s41557-026-02177-8

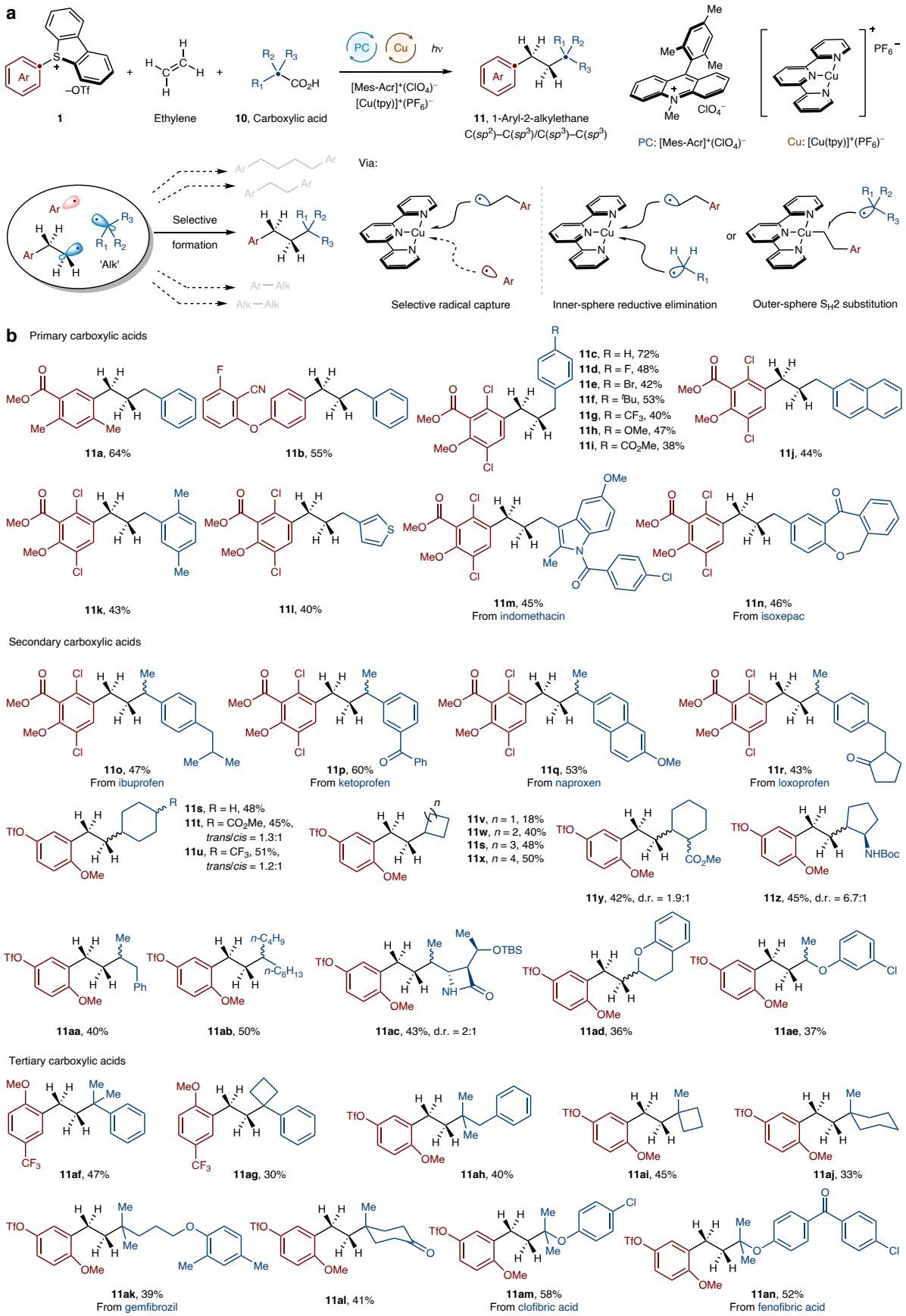

Fig. 5 | Extension of reaction to carboxylic acids as C(sp^3) synthons. a, The copper catalyst selectively promotes the formation of 1-aryl-2-alkylethane from three distinct radicals. **b**, Substrate scope. The reactions were performed under modified standard conditions (Supplementary Section 5.1) and isolated yields are reported. Mes, mesityl; Acr, acridinium; OTBS, *tert*-butyldimethylsilyloxy.

diarylation to yield methyl-substituted 1,2-arylethanes (**13j**–**13n**). In addition, the protocol was successfully extended to unactivated alkenes (**13o** and **13p**), 1,1-disubstituted alkenes (**13q**) and vinyl acetate (**13r**), all of which delivered the desired diarylated products with good efficiency. These results highlight the versatility of the $Cu(tpy)^+$ complex. Beyond primary alkyl radicals, the catalyst also demonstrated excellent reactivity and selectivity towards benzylic, allylic, secondary, tertiary and α-oxy radicals, enabling their effective capture and subsequent functionalization.

Conclusion

We have developed a generalized platform for ethylene 1,2-dicarbofunctionalization that facilitates the rapid construction of a wide range of 1,2-dicarbofunctionalized ethanes encompassing C(sp^3), C(sp^2) and C(*sp*) moieties, valuable scaffolds in pharmaceuticals and natural products. This three-component coupling reaction is enabled by photoredox/copper dual catalysis, in which the copper–tpy complex is critical for modulating the three-component selectivity. Mechanistic investigation uncovered that the strongly π-accepting tpy facilitates a metal–radical polarity-match mechanism that governs the selective capture of nucleophilic alkyl radicals over electrophilic radicals by the copper catalyst. This mechanism is essential to overcome the two-component coupling challenge arising from the inertness of ethylene, expanding its synthetic utility for the construction of value-added molecules. More broadly, this work identifies metal–radical polarity match as a design principle for controlling selectivity in multiradical transformations, based on the recognition that the electronic properties of a ligand can modulate radical capture. This concept provides a structure–activity framework for rational catalyst design in metallaphotoredox chemistry, especially in settings where multiple transient radical intermediates compete for catalyst engagement.

Online content

Any methods, additional references, Nature Portfolio reporting summaries, source data, extended data, supplementary information, acknowledgements, peer review information; details of author contributions and competing interests; and statements of data and code availability are available at https://doi.org/10.1038/s41557-026-02177-8.

References

1. Twilton, J. et al. The merger of transition metal and photocatalysis. *Nat. Rev. Chem.* **1**, 0052 (2017).
2. Chan, A. Y. et al. Metallaphotoredox: the merger of photoredox and transition metal catalysis. *Chem. Rev.* **122**, 1485–1542 (2021).
3. Zhang, J. & Rueping, M. Metallaphotoredox catalysis for sp^3 C–H functionalizations through single-electron transfer. *Nat. Catal.* **7**, 963–976 (2024).
4. Golden, D. L., Suh, S.-E. & Stahl, S. S. Radical C(sp^3)–H functionalization and cross-coupling reactions. *Nat. Rev. Chem.* **6**, 405–427 (2022).
5. Wang, X. et al. Strategies and mechanisms of first-row transition metal-regulated radical C–H functionalization. *Chem. Rev.* **124**, 10192–10280 (2024).
6. Huang, H.-M., Garduño-Castro, M. H., Morrill, C. & Procter, D. J. Catalytic cascade reactions by radical relay. *Chem. Soc. Rev.* **48**, 4626–4638 (2019).
7. Zhang, Z., Chen, P. & Liu, G. Copper-catalyzed radical relay in C(sp^3)–H functionalization. *Chem. Soc. Rev.* **51**, 1640–1658 (2022).
8. Smith, R. T. et al. Metallaphotoredox-catalyzed cross-electrophile C_{sp^3}–C_{sp^3} coupling of aliphatic bromides. *J. Am. Chem. Soc.* **140**, 17433–17438 (2018).
9. Liu, W., Lavagnino, M. N., Gould, C. A., Alcázar, J. & MacMillan, D. W. C. A biomimetic S_H2 cross-coupling mechanism for quaternary sp^3-carbon formation. *Science* **374**, 1258–1263 (2021).
10. Vasilopoulos, A., Krska, S. W. & Stahl, S. S. C(sp^3)–H methylation enabled by peroxide photosensitization and Ni-mediated radical coupling. *Science* **372**, 398–403 (2021).
11. Cai, Q., McWhinnie, I. M., Dow, N. W., Chan, A. Y. & MacMillan, D. W. C. Engaging alkenes in metallaphotoredox: a triple catalytic, radical sorting approach to olefin–alcohol cross-coupling. *J. Am. Chem. Soc.* **146**, 12300–12309 (2024).
12. Chen, R. et al. Alcohol–alcohol cross-coupling enabled by S_H2 radical sorting. *Science* **383**, 1350–1357 (2024).
13. Sarkar, S., Cheung, K. P. S. & Gevorgyan, V. C–H functionalization reactions enabled by hydrogen atom transfer to carbon-centered radicals. *Chem. Sci.* **11**, 12974–12993 (2020).
14. Wang, Y., Bao, Z.-P., Mao, X.-D., Hou, M. & Wu, X.-F. Intermolecular 1,2-difunctionalization of alkenes. *Chem. Soc. Rev.* **54**, 9530–9573 (2025).
15. Ribelli, T., Matyjaszewski, K. & Poli, R. The interaction of carbon-centered radicals with copper(I) and copper(II) complexes. *J. Coord. Chem.* **71**, 1641–1668 (2018).
16. Lin, Q., Spielvogel, E. H. & Diao, T. Carbon-centered radical capture at nickel(II) complexes: spectroscopic evidence, rates, and selectivity. *Chem* **9**, 1295–1308 (2023).
17. Spielvogel, E. H., Yuan, J., Hoffmann, N. M. & Diao, T. Nickel-mediated radical capture: evidence for a concerted inner-sphere mechanism. *J. Am. Chem. Soc.* **147**, 19632–19642 (2025).
18. Campbell, M. W., Compton, J. S., Kelly, C. B. & Molander, G. A. Three-component olefin dicarbofunctionalization enabled by nickel/photoredox dual catalysis. *J. Am. Chem. Soc.* **141**, 20069–20078 (2019).
19. Guo, L., Tu, H.-Y., Zhu, S. & Chu, L. Selective, intermolecular alkylarylation of alkenes via photoredox/nickel dual catalysis. *Org. Lett.* **21**, 4771–4776 (2019).
20. Mega, R. S., Duong, V. K., Noble, A. & Aggarwal, V. K. Decarboxylative conjunctive cross-coupling of vinyl boronic esters using metallaphotoredox catalysis. *Angew. Chem. Int. Ed.* **59**, 4375–4379 (2020).
21. Guo, L. et al. General method for enantioselective three-component carboarylation of alkenes enabled by visible-light dual photoredox/nickel catalysis. *J. Am. Chem. Soc.* **142**, 20390–20399 (2020).
22. Tsymbal, A. V., Bizzini, L. D. & MacMillan, D. W. C. Nickel catalysis via S_H2 homolytic substitution: the double decarboxylative cross-coupling of aliphatic acids. *J. Am. Chem. Soc.* **144**, 21278–21286 (2022).
23. Qi, X., Zhu, L., Bai, R. & Lan, Y. Stabilization of two radicals with one metal: a stepwise coupling model for copper-catalyzed radical–radical cross-coupling. *Sci. Rep.* **7**, 43579 (2017).
24. Großkopf, J., Gopatta, C., Martin, R. T., Haseloer, A. & MacMillan, D. W. C. Generalizing arene C–H alkylations by radical–radical cross-coupling. *Nature* **641**, 112–121 (2025).
25. Parsaee, F. et al. Radical philicity and its role in selective organic transformations. *Nat. Rev. Chem.* **5**, 486–499 (2021).
26. Ruffoni, A., Mykura, R. C., Bietti, M. & Leonori, D. The interplay of polar effects in controlling the selectivity of radical reactions. *Nat. Synth.* **1**, 682–695 (2022).
27. Reaxys. https://www.reaxys.com (Elsevier, accessed 9 July 2025).
28. Wu, X. et al. Applications of "linkers" in fragment-based drug design. *Bioorg. Chem.* **127**, 105921 (2022).
29. Jordan, J. B. et al. Fragment-linking approach using ^{19}F NMR spectroscopy to obtain highly potent and selective inhibitors of β-secretase. *J. Med. Chem.* **59**, 3732–3749 (2016).
30. Drapier, T. et al. Enhancing action of positive allosteric modulators through the design of dimeric compounds. *J. Med. Chem.* **61**, 5279–5291 (2018).

31. Denny, R. A. et al. Structure-based design of highly selective inhibitors of the CREB binding protein bromodomain. *J. Med. Chem.* **60**, 5349–5363 (2017).
32. Fang, W.-S. et al. Discovery of a series of selective and cell permeable beta-secretase (BACE1) inhibitors by fragment linking with the assistance of STD-NMR. *Bioorg. Chem.* **92**, 103253 (2019).
33. Li, J., Luo, Y., Cheo, H. W., Lan, Y. & Wu, J. Photoredox-catalysis-modulated, nickel-catalyzed divergent difunctionalization of ethylene. *Chem* **5**, 192–203 (2019).
34. Ohashi, M., Shirataki, H., Kikushima, K. & Ogoshi, S. Nickel-catalyzed formation of fluorine-containing ketones via the selective cross-trimerization reaction of tetrafluoroethylene, ethylene, and aldehydes. *J. Am. Chem. Soc.* **137**, 6496–6499 (2015).
35. Harper, M. J., Emmett, E. J., Bower, J. F. & Russell, C. A. Oxidative 1,2-difunctionalization of ethylene via gold-catalyzed oxyarylation. *J. Am. Chem. Soc.* **139**, 12386–12389 (2017).
36. Whitehurst, W. G., Kim, J., Koenig, S. G. & Chirik, P. J. Three-component coupling of arenes, ethylene, and alkynes catalyzed by a cationic bis(phosphine) cobalt complex: intercepting metallacyclopentenes for C–H functionalization. *J. Am. Chem. Soc.* **144**, 4530–4540 (2022).
37. Yu, J. et al. Metal-free radical difunctionalization of ethylene. *Chem* **9**, 472–482 (2023).
38. Liu, T. et al. Modular assembly of arenes, ethylene and heteroarenes for the synthesis of 1,2-arylheteroaryl ethanes. *Nat. Chem.* **16**, 1705–1714 (2024).
39. Takano, H. et al. Radical difunctionalization of gaseous ethylene guided by quantum chemical calculations: selective incorporation of two molecules of ethylene. *ACS Omega* **6**, 33846–33854 (2021).
40. Zhang, W. et al. Modular and practical 1,2-aryl(alkenyl) heteroatom functionalization of alkenes through iron/photoredox dual catalysis. *Angew. Chem. Int. Ed.* **62**, e202310978 (2023).
41. Hu, X., Cheng-Sánchez, I., Kong, W., Molander, G. A. & Nevado, C. Nickel-catalysed enantioselective alkene dicarbofunctionalization enabled by photochemical aliphatic C–H bond activation. *Nat. Catal.* **7**, 655–665 (2024).
42. Cao, Z., Chen, F. & Zhu, C. Radical docking–migration: a powerful strategy for difunctionalization of alkenes and alkynes. *Chem. Sci.* **17**, 2913–2931 (2026).
43. Fischer, H. & Radom, L. Factors controlling the addition of carbon-centered radicals to alkenes—an experimental and theoretical perspective. *Angew. Chem. Int. Ed.* **40**, 1340–1371 (2001).
44. Creutz, S. E., Lotito, K. J., Fu, G. C. & Peters, J. C. Photoinduced Ullmann C–N coupling: demonstrating the viability of a radical pathway. *Science* **338**, 647–651 (2012).
45. Johnson, M. W., Hannoun, K. I., Tan, Y., Fu, G. C. & Peters, J. C. A mechanistic investigation of the photoinduced, copper-mediated cross-coupling of an aryl thiol with an aryl halide. *Chem. Sci.* **7**, 4091–4100 (2016).
46. Neufeldt, S. R. & Sanford, M. S. Combining transition metal catalysis with radical chemistry: dramatic acceleration of palladium-catalyzed C–H arylation with diaryliodonium salts. *Adv. Synth. Catal.* **354**, 3517–3522 (2012).
47. Li, J. et al. Photoredox catalysis with aryl sulfonium salts enables site-selective late-stage fluorination. *Nat. Chem.* **12**, 56–62 (2020).
48. Kweon, J., Kim, D., Kang, S. & Chang, S. Access to β-lactams via iron-catalyzed olefin oxyamidation enabled by the π-accepting phthalocyanine ligand. *J. Am. Chem. Soc.* **144**, 1872–1880 (2022).
49. Gilbert, M. M. et al. Ligand–metal cooperation enables net ring-opening C–C activation/difunctionalization of cyclopropyl ketones. *ACS Catal.* **13**, 11277–11290 (2023).
50. Huang, Z., Akana, M. E., Sanders, K. M. & Weix, D. J. A decarbonylative approach to alkylnickel intermediates and $C(sp^3)$–$C(sp^3)$ bond formation. *Science* **385**, 1331–1337 (2024).
51. Berger, F. et al. Site-selective and versatile aromatic C–H functionalization by thianthrenation. *Nature* **567**, 223–228 (2019).
52. Wang, F., Wang, D., Mu, X., Chen, P. & Liu, G. Copper-catalyzed intermolecular trifluoromethylarylation of alkenes: mutual activation of arylboronic acid and CF_3^+ reagent. *J. Am. Chem. Soc.* **136**, 10202–10205 (2014).
53. Pal, S., Cotard, M., Gérardin, B., Hoarau, C. & Schneider, C. Cu-catalyzed oxidative allylic C–H arylation of inexpensive alkenes with (hetero)aryl boronic acids. *Org. Lett.* **23**, 3130–3135 (2021).
54. Zhang, Z., Tilby, M. J. & Leonori, D. Boryl radical-mediated halogen-atom transfer enables arylation of alkyl halides with electrophilic and nucleophilic coupling partners. *Nat. Synth.* **3**, 1221–1230 (2024).
55. Aukland, M. H., Šiaučiulis, M., West, A., Perry, G. J. P. & Procter, D. J. Metal-free photoredox-catalysed formal C–H/C–H coupling of arenes enabled by interrupted Pummerer activation. *Nat. Catal.* **3**, 163–169 (2020).
56. Winter, A., Newkome, G. R. & Schubert, U. S. Catalytic applications of terpyridines and their transition metal complexes. *ChemCatChem* **3**, 1384–1406 (2011).
57. Jaganyi, D., Hofmann, A. & van Eldik, R. Controlling the lability of square-planar Pt^{II} complexes through electronic communication between π-acceptor ligands. *Angew. Chem. Int. Ed.* **40**, 1680–1683 (2001).
58. Hofmann, A., Jaganyi, D., Munro, O. Q., Liehr, G. & van Eldik, R. Electronic tuning of the lability of Pt(II) complexes through π-acceptor effects. Correlations between thermodynamic, kinetic, and theoretical parameters. *Inorg. Chem.* **42**, 1688–1700 (2003).
59. Czap, A., Heinemann, F. W. & van Eldik, R. Influence of terpyridine as π-acceptor ligand on the kinetics and mechanism of the reaction of NO with ruthenium(III) complexes. *Inorg. Chem.* **43**, 7832–7843 (2004).
60. Le, C., Chen, T. Q., Liang, T., Zhang, P. & MacMillan, D. W. C. A radical approach to the copper oxidative addition problem: trifluoromethylation of bromoarenes. *Science* **360**, 1010–1014 (2018).
61. Hazra, A., Lee, M. T., Chiu, J. F. & Lalic, G. Photoinduced copper-catalyzed coupling of terminal alkynes and alkyl iodides. *Angew. Chem. Int. Ed.* **57**, 5492–5496 (2018).
62. Li, Z., Torres-Ochoa, R. O., Wang, Q. & Zhu, J. Functionalization of remote $C(sp^3)$–H bonds enabled by copper-catalyzed coupling of *O*-acyloximes with terminal alkynes. *Nat. Commun.* **11**, 403 (2020).
63. Zeng, X. et al. Aryl radical enabled, copper-catalyzed Sonogashira-type cross-coupling of alkynes with alkyl iodides. *ACS Catal.* **13**, 2761–2770 (2023).
64. Lovering, F. Escape from Flatland 2: complexity and promiscuity. *Med. Chem. Commun.* **4**, 515–519 (2013).
65. Kranthikumar, R. Recent advances in $C(sp^3)$–$C(sp^3)$ cross-coupling chemistry: a dominant performance of nickel catalysts. *Organometallics* **41**, 667–679 (2022).
66. Liang, H. & Morken, J. P. Direct observation of alkyl group transmetalation from boron to copper: impact of structure modification and the critical role of copper–oxygen preassociation in stereospecificity. *J. Am. Chem. Soc.* **147**, 13126–13130 (2025).
67. Mondal, S., Mandal, S., Mondal, S., Midya, S. P. & Ghosh, P. Photocatalytic decarboxylation of free carboxylic acids and their functionalization. *Chem. Commun.* **60**, 9645–9658 (2024).

Methods

Typical procedure for photoredox/copper dual-catalysed 1,2-dicarbofunctionalization of ethylene

To a 10-ml oven-dried microwave tube fitted with a magnetic stir bar was added $Ru(DMB)_3(PF_6)_2$ (1.9 mg, 0.0020 mmol, 0.02 equiv.), tpy (2.8 mg, 0.012 mmol, 0.12 equiv.), aryl-DBT salt (0.10 mmol, 1.0 equiv.) and arylboronic acid (0.20 mmol, 2.0 equiv.). The tube was then transferred into an argon-filled glove box and $Cu(MeCN)_4(PF_6)$ (3.7 mg, 0.010 mmol, 0.10 equiv.), K_3PO_4 (42 mg, 0.20 mmol, 2.0 equiv.) and 4-Å molecular sieves (50 mg) were added, followed by anhydrous MeCN (0.8 ml), *t*BuCN (0.80 ml) and *t*BuOAc (0.40 ml). The tube was then sealed with a Synthware 14/20 threaded tight-seal flange rubber septum and removed from the glove box.

The septum was further sealed with strong adhesive electric tape. The mixture was sparged with a balloon filled with ethylene through a long stainless-steel needle (~1 min), after which 60 ml ethylene was introduced into the tube through a syringe by immersing the tube in liquid nitrogen, causing the ethylene (boiling point −103.7 °C) to condense. The top of the septum was immediately sealed with another piece of electric tape and parafilm after the removal of the syringe. After slowly returning to room temperature, the tube (pressure ~5 atm) was irradiated with a 40-W, 456-nm blue lamp with stirring for 24 h and an overhead fan cooling.

After irradiation, the tube was vented with a needle before the septum was removed. The reaction mixture was diluted with Et_2O and passed through a silica pad. The resulting solution was concentrated and the crude mixture was purified by flash column chromatography to obtain the desired product.

Data availability

All of the data supporting the findings of this study are available within the article and its Supplementary Information.

Acknowledgements

We thank H. T. Ang (NUS) for helpful scientific discussion and substantial contributions to manuscript writing and editing. We thank K. L. Wong (NUS) for help with HRMS experiments. We are grateful for the financial support provided by the SUSTech-NUS Joint Research Program, Ministry of Education (MOE) of Singapore (T2EP10224-0005), the National Research Foundation, the Prime Minister's Office of Singapore, under its NRF-CRP Programme (NRFCRP25-2020RS-0002), the National Natural Science Foundation of China (22371200) and the NUS (Suzhou) Research Institute, Science and Technology Project of Jiangsu Province (BZ2022056).

Author contributions

Z.L. and J.W. conceived the project. Z.L. developed the system and conducted most of the experimental work. Z.L. and C.W. conducted the computational study. A.W., T.L. and W.Z. assisted with the experiments. Z.D., W.Z. and J.W. supervised and coordinated the project. Z.L., Z.D., W.Z. and J.W. wrote the paper with input from all the authors.

Competing interests

The authors declare no competing interests.

Additional information

Extended data is available for this paper at https://doi.org/10.1038/s41557-026-02177-8.

Supplementary information The online version contains supplementary material available at https://doi.org/10.1038/s41557-026-02177-8.

Correspondence and requests for materials should be addressed to Zhe Dong, Weigang Zhang or Jie Wu.

Peer review information *Nature Chemistry* thanks Jesus Alcazar and the other, anonymous, reviewer(s) for their contribution to the peer review of this work.

https://doi.org/10.1038/s41557-026-02177-8

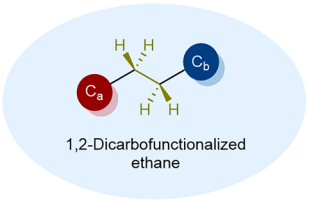

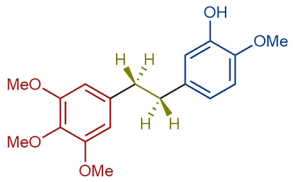
Erianin, from Dendrobium chrysotoxum Lindl anti-cancer & anti-bacterial

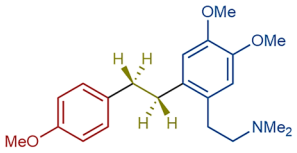
Polysignine, from Polyalthia insignis

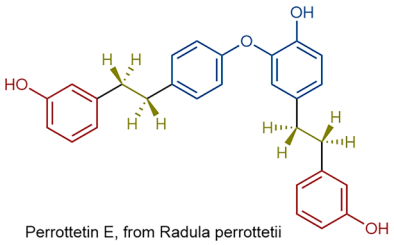
Perrottetin E, from Radula perrottetii

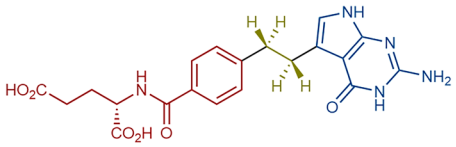
Pemetrexed, chemotherapy agent for pleural mesothelioma and non-small cell lung cancer (NSCLC)

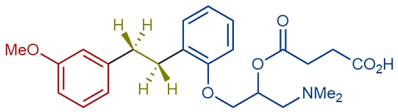
Sarpogrelate, serotonin 5-HT_{2A}, 5-HT_{2B} and 5-HT_{2C} receptor antagonist

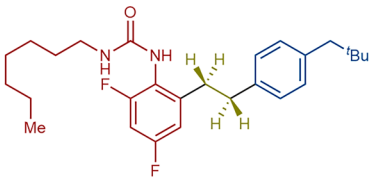
447C88, acyl-coenzyme A:cholesterol acyltransferase (ACAT) Inhibitor

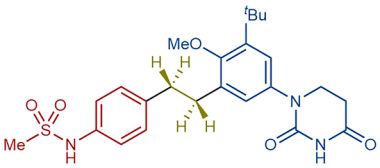
Hepatitis C Virus NS5B Polymerase inhibitor

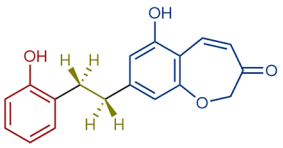
Radstrictin I, from Radula constricta cytotoxic agent by mitochondria-derived paraptosis

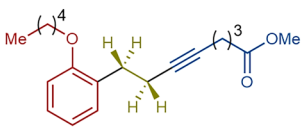
Peroxisome proliferator-activated receptor (PPAR) nuclear receptor activator

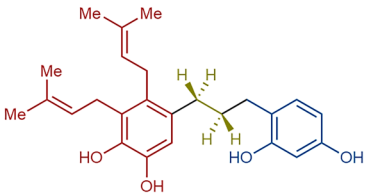
Kazinol F, from Broussonetia papyrifera antioxidant, tyrosinase inhibitor

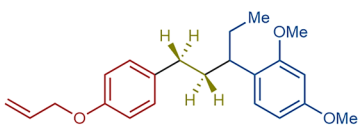
Nyasol derivative with saturated ethane linker antimalaria and antiplamoidal agent

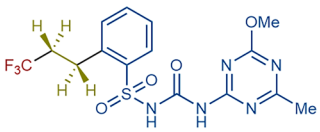
Prosulfuron, broad-spectrum herbicide

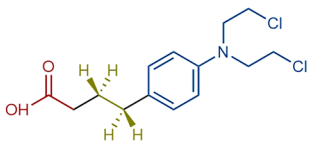
Chlorambucil, chemotherapy agent for chronic lymphocytic leukemia (CLL)

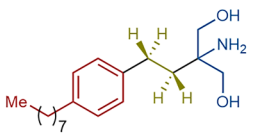
Fingolimod, immunomodulating agent for treatment of multiple sclerosis

Extended Data Fig. 1 | Bioactive molecules and natural products encompassing 1,2-dicarbofunctionalized ethane motif. 1,2-Dicarbofunctionalized ethanes are prevalent motifs in medicinal relevant molecules, some selected examples bearing alkyl (sp^3), (hetero)aryl (sp^2), and alkynyl (sp) carbogenic functional groups are shown. *t*Bu, tert-butyl. OMe, methoxy.

https://doi.org/10.1038/s41557-026-02177-8

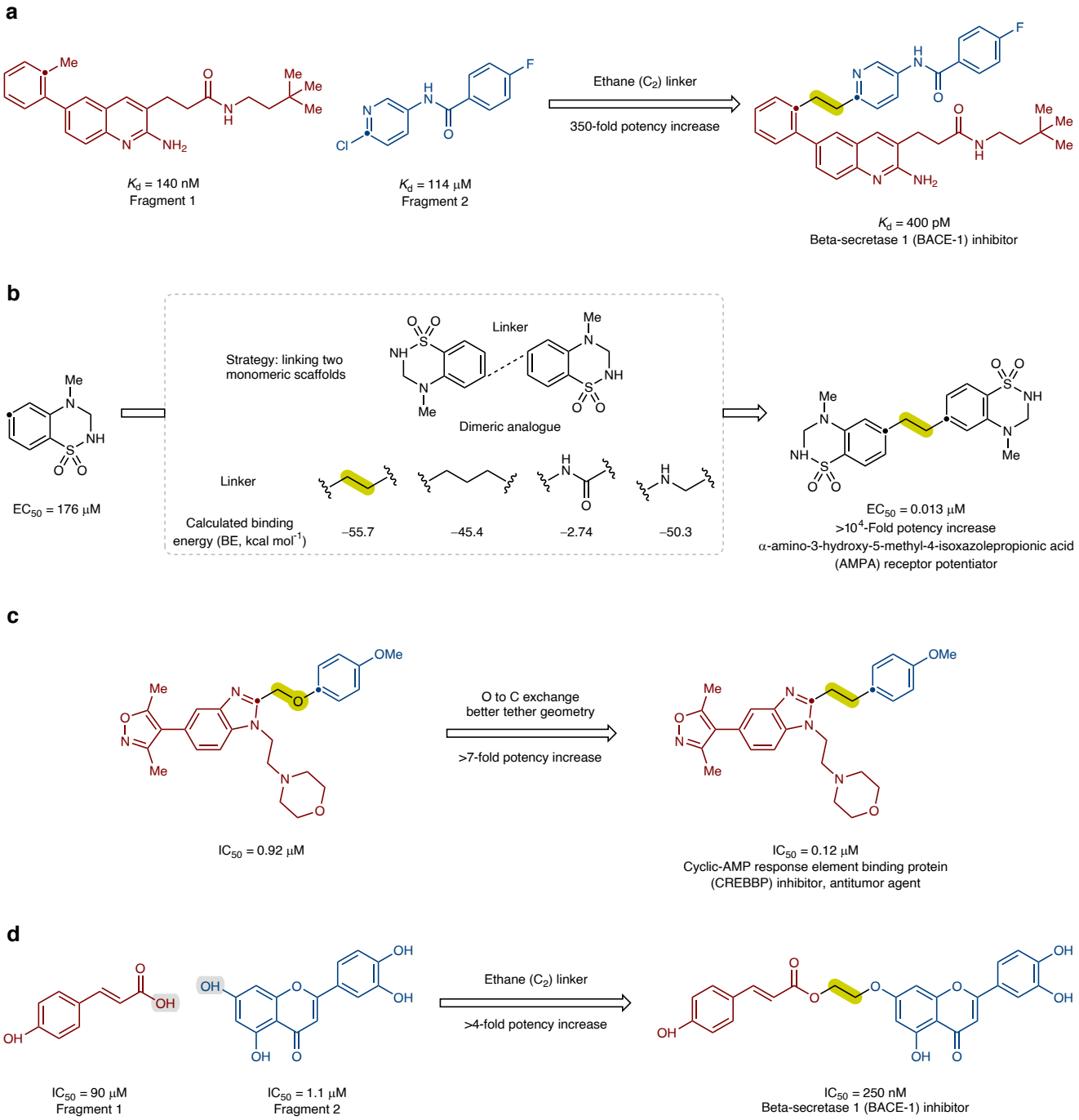

Extended Data Fig. 2 | Ethane (C2) bridge represents an important motif in fragment-based drug design (FBDD). a, Linking two aryl moieties with an ethane bridge allowed the discovery of potent and selective BACE-1 inhibitor with 350-fold potency boost[29]. **b**, Dimerized 1,2,4-benzothiadiazine 1,1-dioxide (BTD)-type AMPA potentiator linked by an ethane bridge showed over 10^4 potency boost[30]. **c**, Changing the ether linker in a CREBBP inhibitor to the corresponding ethane linker resulted in over 7-fold potency boost[31]. **d**, Linking the ester and phenol functional group with an ethane bridge allowed for an over 4-fold potency boost in the search for BACE-1 inhibitor[32]. K_d, dissociation constant; EC_{50}, half maximal effective concentration; IC_{50}, half maximal inhibitory concentration; OMe, methoxy.

https://doi.org/10.1038/s41557-026-02177-8

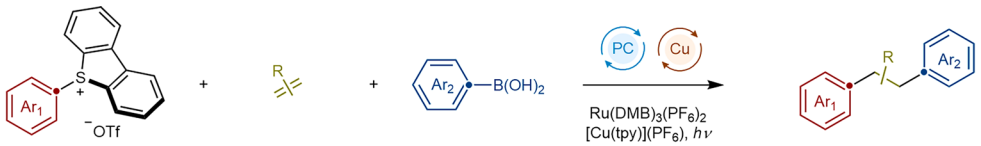

1 **12**, Substituted alkenes or 1,3-diene **2** **13**

From styrene

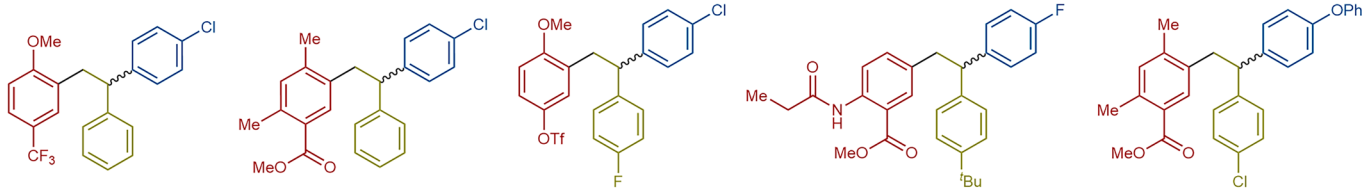

13a, 77% **13b**, 80% **13c**, 67% **13d**, 40% **13e**, 55%

From 1,3-butadiene

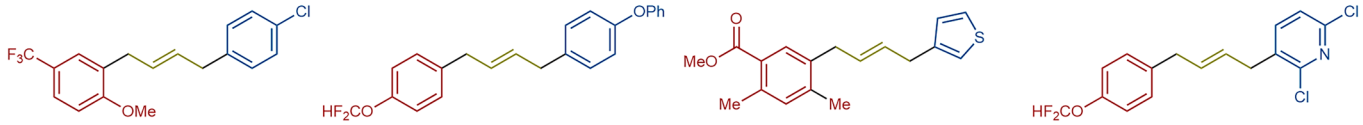

13f, 72%, E/Z > 20:1 **13g**, 70%, E/Z > 20:1 **13h**, 63%, E/Z > 20:1 **13i**, 55%, E/Z > 20:1

From propylene

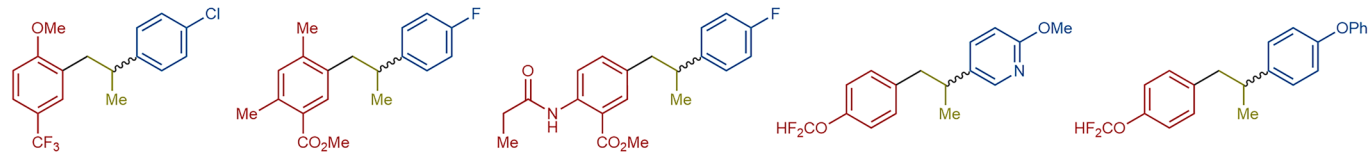

13j, 58% **13k**, 60% **13l**, 46% **13m**, 55% **13n**, 58%

From other alkenes

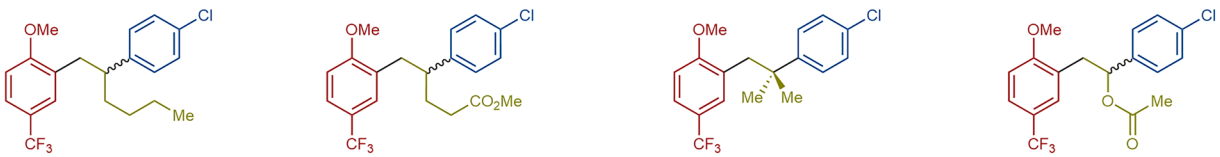

13o, 48% from 1-hexene **13p**, 50% from methyl 4-penteonate **13q**, 34% from isobutene **13r**, 47% from vinyl acetate

Extended Data Fig. 3 | Application of photoredox/copper dual-catalyzed ethylene 1,2-diarylation to substituted alkenes and 1,3-dienes. Beyond ethylene, the 1,2-diarylation protocol can be applied to other unsaturated systems, such as subtituted alkene, 1,3-diene, and propylene, another gaseous feedstock chemical. $^{-}$OTf, trifluoromethanesulfonate; PC, photocatalyst; Ar, aryl; DMB, 4,4′-dimethyl-2,2′-bipyridine; OMe, methoxy; OPh, phenoxy; OTf, trifluoromethanesulfonyloxy; *t*Bu, tert-butyl.

https://doi.org/10.1038/s41557-026-02177-8

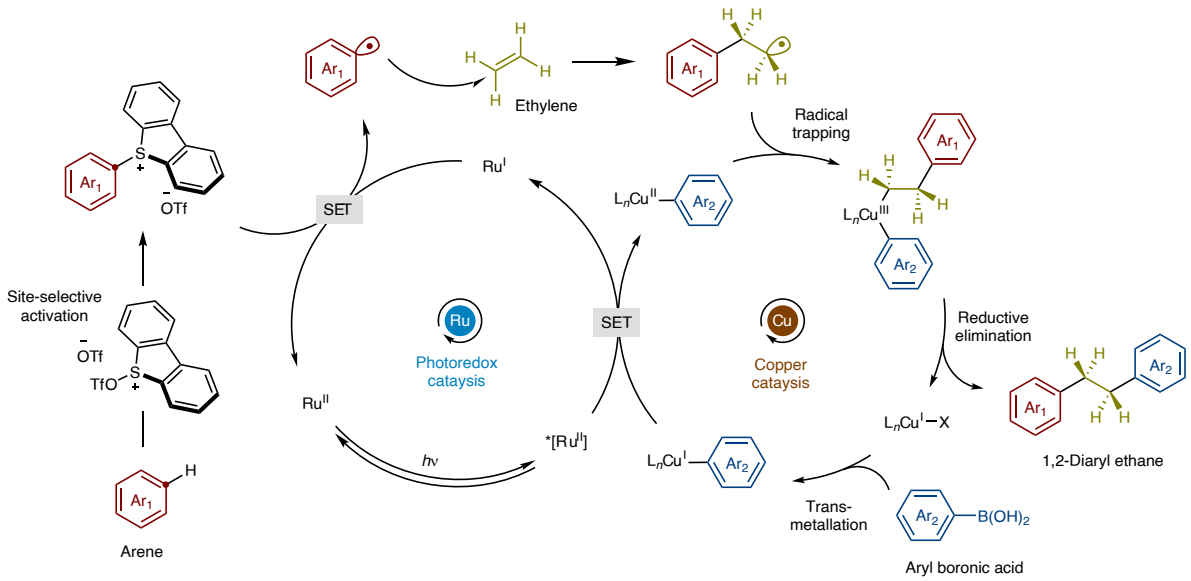

Extended Data Fig. 4 | Proposed mechanisms of photoredox/copper dual-catalyzed 1,2-diarylation of ethylene. The Ru-based photocatalyst operates through a reductive quenching cycle, in which single-electron transfer from the Cu(I) catalyst to the excited-state Ru(II)* species generates ground-state Ru(I). The resulting Ru(I) species reduces the aryl-DBT salt, releasing an aryl radical that undergoes radical addition followed by capture by the copper catalyst. The resulting transient Cu(III) species rapidly undergoes reductive elimination to afford the 1,2-diarylethane product. SET, single electron transfer; $^{-}$OTf, trifluomethanesulfonate; Ar, aryl; X, ligand; L, ligand; PC, photocatalyst; TfO, trifluoromethanesulfonyloxy.

https://doi.org/10.1038/s41557-026-02177-8

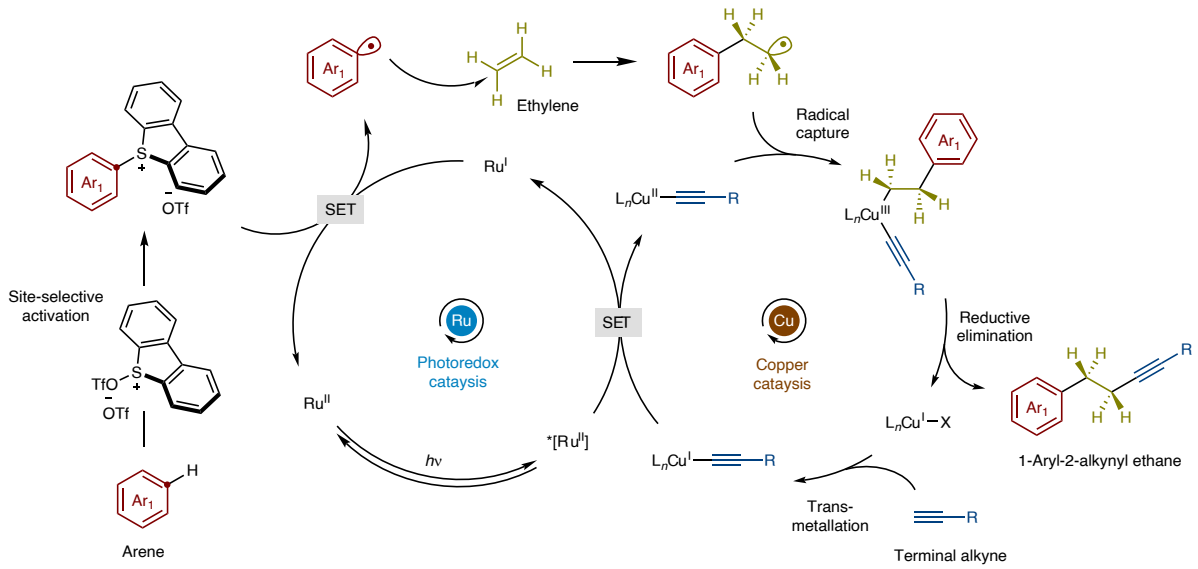

Extended Data Fig. 5 | Proposed mechanisms of photoredox/copper dual-catalyzed 1-aryl-2-alkynylation of ethylene. The Ru-based photocatalyst operates through a reductive quenching cycle, in which single-electron transfer from the Cu(I) catalyst to the excited-state Ru(II)* species generates ground-state Ru(I). The resulting Ru(I) species reduces the aryl-DBT salt, releasing an aryl radical that undergoes radical addition followed by capture by the copper catalyst. The resulting transient Cu(III) species rapidly undergoes reductive elimination to afford the 1-aryl-2-alkynylethane product. SET, single electron transfer; $^{-}$OTf, trifluomethanesulfonate; Ar, aryl; X, ligand; L, ligand; R, functional group; PC, photocatalyst; TfO, trifluoromethanesulfonyloxy.

https://doi.org/10.1038/s41557-026-02177-8

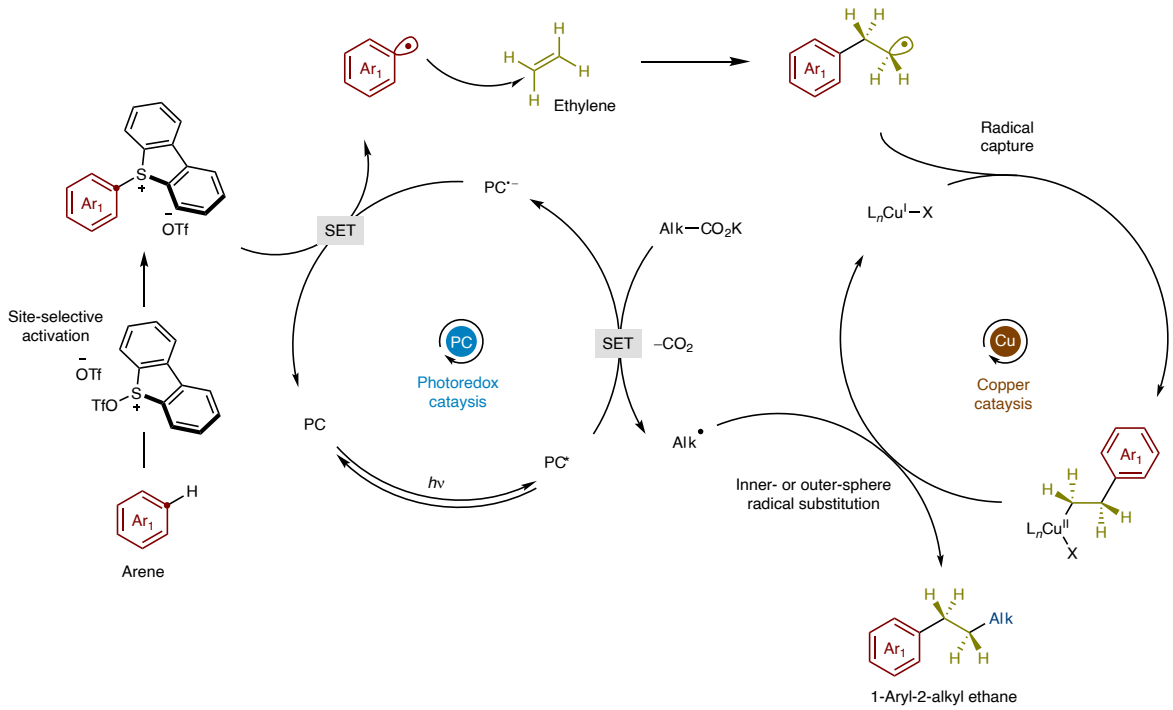

Extended Data Fig. 6 | Proposed mechanisms of photoredox/copper dual-catalyzed 1-aryl-2-alkylation of ethylene. The acridinium-based photocatalyst operates through a reductive quenching cycle, in which single-electron transfer from the carboxylate to the excited-state photocatalyst generates the ground-state reduced photocatalyst. This reduced species then reduces the aryl-DBT salt, releasing an aryl radical that undergoes radical addition followed by capture by the copper catalyst. The alkyl radical generated by decarboxylation subsequently couples with the copper species bearing the primary alkyl group, through either an inner- or outer-sphere pathway, to afford the 1-aryl-2-alkylethane product. SET, single electron transfer; $^{-}$OTf, trifluomethanesulfonate; Ar, aryl; X, ligand; L, ligand; Alk, alkyl; PC, photocatalyst; TfO, trifluoromethanesulfonyloxy.